Journal Pre-proof

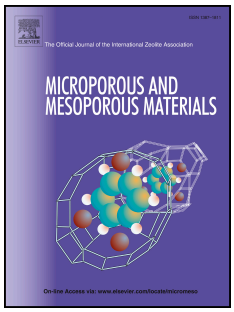

Substitution of Cetyltrimethylammonium for OSDA Cations During B-SSZ-70 Zeotype Synthesis and Its Influence on Delamination

Maya Ramamurthy, Nicolás A. Grosso-Giordano, Son-Jong Hwang, Le Xu, Dan Xie, Manish Mishra, Alexander Okrut, Stacey Zones, Alexander Katz

PII: S1387-1811(21)00168-2

DOI: https://doi.org/10.1016/j.micromeso.2021.111042

Reference: MICMAT 111042

To appear in: *Microporous and Mesoporous Materials*

Received Date: 6 January 2021

Revised Date: 8 March 2021

Accepted Date: 12 March 2021

Please cite this article as: M. Ramamurthy, Nicolá.A. Grosso-Giordano, S.-J. Hwang, L. Xu, D. Xie, M. Mishra, A. Okrut, S. Zones, A. Katz, Substitution of Cetyltrimethylammonium for OSDA Cations During B-SSZ-70 Zeotype Synthesis and Its Influence on Delamination, *Microporous and Mesoporous Materials* (2021), doi: https://doi.org/10.1016/j.micromeso.2021.111042.

Credit statements:

M.R., A.O., L.X., N.G., M.M., S.H. and D.X.: Investigation
M.R., A.O.: Visualization
M.R.: Writing – Original Draft
M.R., L.X., A.O., S.Z., A.K.: Writing – Review & Editing
A.O., A.K., S.Z.: Conceptualization, Supervision

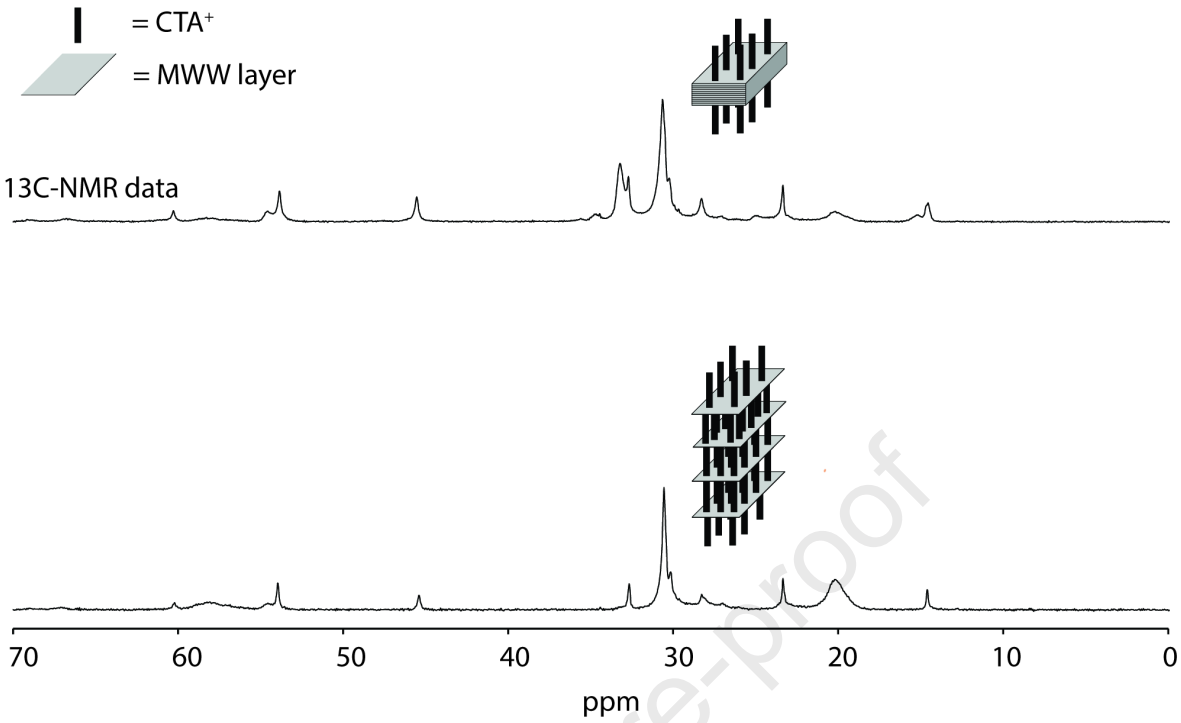

Substitution of Cetyltrimethylammonium for OSDA Cations During B-SSZ-70 Zeotype Synthesis and Its Influence on Delamination

Maya Ramamurthy[1], Nicolás A. Grosso-Giordano[1], Son-Jong Hwang[2], Le Xu[1], Dan Xie[3], Manish Mishra[1], Alexander Okrut[*,4], Stacey Zones[*,3], Alexander Katz[*,1]

[1]Department of Chemical and Biomolecular Engineering, University of California, Berkeley, Berkeley, California 94720, United States

[2]Division of Chemistry and Chemical Engineering, California Institute of Technology, Pasadena, California 91125, USA

[3]Chevron Energy Technology Company, Richmond, California 94804, United States

[4]Berkeley Materials Solutions, LLC, Richmond, California 94803, United States

Abstract

We investigated the substitution of structure-directing agent diisobutylimidazolium hydroxide with cetyltrimethylammonium hydroxide (CTA^+OH^-) surfactant in the synthesis gel of layered-zeotype-precursor B-SSZ-70(P). At low substitution levels, CTA^+ interacts with the external-zeotype surface, where it assembles. At higher surfactant amounts, CTA^+ intercalation occurs, leading to swelling of the precursor material, as evidenced by powder X-ray diffraction. Characterization of adsorbed CTA^+ cations by ^{13}C MAS NMR spectroscopy demonstrates unique broad resonances in the intercalated layers, which represent a more rigid environment than in the external-surface assemblies. At still higher CTA^+ substitution levels in the synthesis gel, we observe the formation of amorphous mesoporous silica. We attempted to delaminate materials synthesized with varying CTA^+ substitution levels using mild conditions, in which the conventional sonication step is replaced with an easy-to-scale high-shear mixing, and in which the use of halide reagents, which are corrosive and have been required in the past, is also avoided. Our data demonstrate that synthesis of a swollen material *per se* is not essential as an intermediate for delamination, and that layered zeolite precursor swelling can actually undermine zeolite delamination. Our results instead point to the CTA^+ external-surface assemblies as facilitating ease of SSZ-70 delamination under these mild conditions. When calcined and functionalized with grafted titanium centers, the delaminated materials are highly active and selective olefin epoxidation catalysts with organic hydroperoxides, showing a 40% higher epoxide conversion than a catalyst prepared from conventional B-SSZ-70.

Introduction

The synthesis of zeotype catalysts with high external surface areas is motivated by the need to circumvent internal-diffusion limitations and enable access to catalytically active sites at the pore mouth for bulky reactants.[1–5] Among the several approaches that have been developed for the synthesis of such catalysts,[6–12] the delamination of layered zeolite precursors represents a promising route.[13–20] Much of our work has focused on delamination of layered zeotype precursor B-SSZ-70(P), which has found application as a material for synthesizing crystalline supports for catalysis.[20–23] The recalcitrance of the SSZ-70(P) framework to delamination has been a significant challenge, when compared with other layered zeolite precursors, such as ERB-1, which can be delaminated by a simple $Zn(NO_3)_2$ or $Al(NO_3)_3$ treatment.[19,24] We have ascribed this greater difficulty of SSZ-70(P) delamination to be the result of its cationic organic structure directing agent (OSDA), in contrast to the neutral OSDA used for synthesis of ERB-1. This cationic OSDA results in greater (e.g., electrostatic) interactions with the negatively charged zeotype surface relative to the weaker hydrogen-bonding interactions between neutral OSDA and the surface in ERB-1. While there has been recent progress in SSZ-70(P) delamination that successfully circumvents the need for difficult-to-scale ultrasonication, by using post-synthetic treatment with Zn^{2+},[20,25] corrosive and environmentally unfriendly halide-containing reagents (e.g., fluoride salts) continue to be required for SSZ-70(P) delamination, as they have been since the development of delamination synthetic approaches that preserve the crystalline integrity of the crystalline framework.[18,26]

Our hypothesis is that thinner zeotype precursor crystallites will facilitate faster (and therefore kinetically easier) layer separation via delamination, as there are fewer interlayer bonds to break for separating any two precursor crystallites. To investigate this, we aimed to limit B-SSZ-70(P) crystallite growth, as illustrated schematically in Figure 1. The underpinnings of this strategy rely on decreasing surface free energy by capping the external surface with CTA^+ cations, which are known to strongly interact with silicate surfaces.[27–32] The addition of CTA^+ to zeolite syntheses has been reported previously for MFI,[33,34] and related CTA^+-promoted growth of small zeolite crystallites has been previously demonstrated for the synthesis of Na-A,[35] CHA,[36] MOR,[37] MFI,[38–41] and MWW.[12,42] However, to the best of our knowledge, the systematic substitution of CTA^+OH^- for $OSDA^+OH^-$ has not been investigated previously,

and inclusion of CTA^+ in the zeolite synthesis has not been investigated previously for facilitating zeotype delamination.

We substituted cetyltrimethylammonium (CTA^+) for $OSDA^+$ cations in the B-SSZ-70(P) synthesis gel, and investigate $OSDA^+$ as a combination with CTA^+, by changing the relative proportions of each, while keeping the total added OH^- amount nearly fixed (at 0.040 ± 0.002 moles in the synthesis gel). Our rationale in synthesizing these materials is based on a possible dual role of CTA^+ in the zeolite synthesis gel, consisting of swelling[15–17,43,44] and limiting the growth of zeotype precursors through self-assembly of nanocrystallites around CTA^+ surfactant assemblies on the external surface. The self-assembly of CTA^+ cations on silicate external surfaces under alkaline conditions typical of zeotype synthesis is well established.[27–32] We hypothesized that these assemblies could occur at relatively low substitution levels in our B-SSZ-70 syntheses, based on reports for MFI synthesis gels to which CTAOH has been added.[40] At longer crystallization times, these assemblies for MFI synthesis later gave way to fully encapsulated CTA^+ within the zeolite.[40] We thus hypothesized (i) at low amounts of added CTA^+ in the synthesis gel, kinetics dictates synthesis of crystallites that are terminated by CTA^+ groups bound to deprotonated silanols at the crystallite external surface, and (ii) at higher proportions of added CTA^+ in the synthesis gel, in addition to (i), CTA^+-swelling of zeotype layers occurs during synthesis, as illustrated in Figure 2.

We characterized the resulting materials using powder X-ray diffraction (PXRD), solid-state ^{13}C MAS NMR spectroscopy, N_2 physisorption at 77 K, and elemental analysis. Following synthesis, we investigated delamination of the resulting layered precursor materials by high-shear mixing, and evaluated the resulting calcined delaminated materials as catalysts, after supporting catalytically active Ti sites on them. We used catalysis as an additional reporter of the extent of delamination, above and beyond the other techniques mentioned above, particularly N_2 physisorption, because previous work directly correlated these two.[22,23] The understanding gained here of the effect of CTAOH added as a substitute for OSDAOH to the zeotype synthesis gel, and its effect on delamination, has broader ramifications related to synthesis and delamination of other layered-zeolite precursors (e.g., ERB-1, MCM-22(P)).[18,24,45,46]

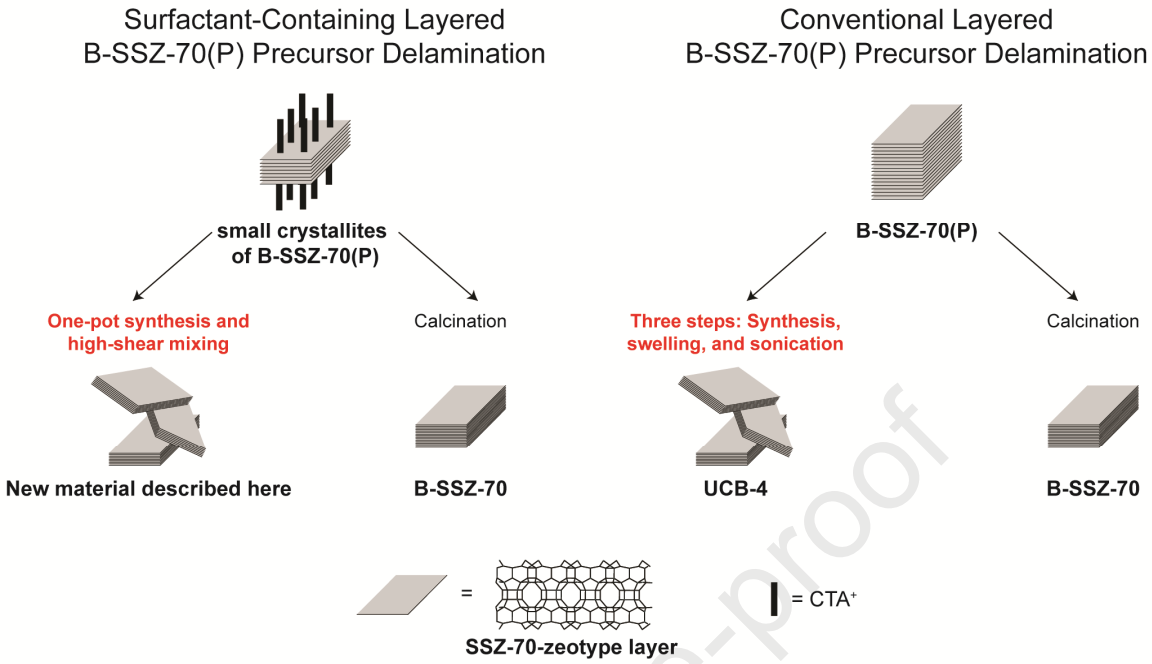

Figure 1. A schematic comparison of the delamination method presented in this work and the conventional delamination method that uses sonication.

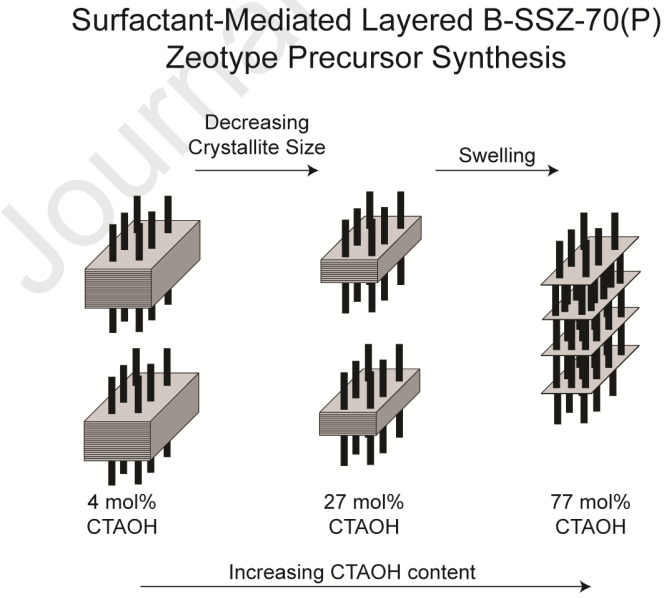

Figure 2. A central hypothesis of this work is that the location of added CTA^+ cations to the synthesis gel can be controlled by their relative proportion when substituting for $OSDA^+$. At low substitution levels, termination of the external-zeotype surface occurs through binding of CTA^+

assemblies to the crystallite external surface area, leading to smaller crystallite thicknesses. Swelling ocurs only at higher substitution levels of CTA^+.

Experimental

Materials

All reagents were reagent-grade quality and were used as received unless otherwise noted. Syntheses of materials B-SSZ-70 and UCB-4 were performed as previously described.[18]

Synthesis of CTAOH-containing materials

A series of B-SSZ-70(P) zeotypes was synthesized by substituting $OSDA^+OH^-$ with CTA^+OH^- while maintaining an approximately fixed total hydroxide amount in the synthesis gels ($n_{CTAOH}/(n_{(CTAOH + OSDA)}$) between 4 mol% and 100 mol% – see Table S1, Supporting Information) This was performed under the constraint that the total combined amount of CTAOH and SDA was fixed at approximately 0.040 ± 0.002 moles. The synthesis gels were prepared by combining suitable amounts of a 10 wt.% solution of CTAOH in water and a 9 wt.% solution of diisobutylimidazolium hydroxide (DIBI) in water with a gel containing 1.2 g of Aerosil-200 silica gel, 2 g of an aqueous 1 M NaOH solution, 0.09 g H_3BO_3, and 0.35 g B-SSZ-70(P) precursor as seed crystals. For example, the gel containing 19 mol% CTAOH was prepared by adding 2 g CTAOH (10 wt.% in water) and 6.32 g of diisobutylimidazolium hydroxide (9 wt.% in water). The resulting mixture had a molar composition of 1.0 SiO_2 : 0.144 SDA : 0.033 CTAOH : 0.100 NaOH : 28.3 H_2O : 0.073 H_3BO_3. A summary of all gel compositions can be found in Table S1. The gels were transferred to a 22 mL Teflon liner and tumbled in a stainless-steel autoclave at 150-155 °C and 60 rpm for 6 days. The reaction mixture was then removed from the autoclave, filtered at room temperature, washed thoroughly with deionized water, and dried at 60°C overnight.

High-shear mixing

Materials were made into a wet paste for high-shear mixing by adding approximately 15 mL of water to 2.5 g of as-synthesized material and centrifuging at 8000 rpm for 5 min. The supernatant was decanted, and the remaining wet paste was high-shear mixed using a dual asymmetric centrifugation mixer (DAC 150.1 FVZ SpeedMixer) from Flack Tec, Inc. according to the following procedure. 0.75-1.25 g of the material paste was placed in a 10 g max cup material holder with two cylindrical zirconium beads (d = 9.5 mm, l = 10 mm). Materials were high-shear mixed for 2 min at 2500 rpm, after which 100 μL of deionized water was added to the material, which was then high-shear mixed again under the same conditions. 10 μL of 1 M NH_4OH was added to the material, and the resulting slurry was high-shear mixed for 1 min at 1700 rpm. The materials were then dried overnight at 60°C and calcined in air at 550°C for 5 hours.

Titanium grafting

Materials were prepared for olefin epoxidation catalysis by replacing framework boron atoms with titanium atoms. Materials were deboronated by adding 20 mL of 2 N HNO_3 to 1 g of material and stirring at 135°C in a high-pressure glass flask for 16 hours. The solid materials were collected on a filter, washed once with 2 N HNO_3, and then washed three times with deionized water. The deboronation step was omitted for the amorphous SiO_2 material. After drying at 150°C for at least two hours, the material (deboronated zeotype or SiO_2 (Selecto silica gel, particles size 32-63 μm)) was functionalized with Ti by adding 4 mL of Titanium(IV)-n-butoxide ($Ti(BuO_4)$) to 0.5 g of material under nitrogen flow. The resulting mixture was stirred at 135°C for one hour. After cooling to room temperature, the suspension was filtered under nitrogen atmosphere and washed multiple times with 1-butanol. The materials were dried at 150°C and then calcined at 550°C for 5 hours.

Characterization methods

A Perkin Elmer 2400 Series II combustion analyzer was used to determine the carbon, hydrogen, and nitrogen (CHN) content of materials. Powder X-ray diffraction (PXRD) patterns were collected on a Bruker GADDS D-8 diffractometer using Cu Kα radiation. Data were collected in the 2θ range from 3° to 30° with a step size of 0.02° and a dwell time of 2 s. Nitrogen physisorption isotherms were measured on a Micromeritics ASAP 2020 instrument at

77 K and materials were evacuated at 350°C for 4 h prior to measurement. External surface area for materials was determined using the t-plot method. Pore size distribution was obtained from density functional theory, assuming a slit pore model and N_2 at 77 K. Diffuse reflectance ultraviolet-visible (DR-UV-Vis) spectroscopy for solid materials was performed on a Cary 400 spectrophotometer (Varian) using polytetrafluoroethylene as a standard. Materials were measured with an average time of 0.166 s and a wavelength data interval of 0.5 nm (180.7 nm min^{-1} scan rate) and results were converted into Kubelka–Munk (F(R)) pseudoabsorbance units. The Ti-content of materials was determined using liquid-phase UV-Vis spectroscopy as follows: Ti extraction was performed by adding 1 mL of H_2SO_4 to approximately 20 mg of solid material in a 10 mL volumetric flask. After 1 hour, a few drops of water were added, followed by 110 μL of H_2O_2, and the flask was filled to 10 mL with water. The solution was passed through a 0.2 μm syringe filter, and the UV-Vis absorbance was measured using a Varian Cary 400 UV-Vis spectrometer. The concentration of Ti in the solution was determined using the absorbance at 408 nm using a previously established calibration curve. SEM images were captured with an acceleration voltage of 10 kV on a Hitachi S-5000 microscope.

Olefin epoxidation catalysis in a batch reactor

Nano-Scale Batch Reaction

0.005 g of catalyst was added to a 5 mL scintillation vial and dried at 150°C for at least 1 h. The vial was then cooled to 70°C and the reaction was started by adding 2.260 mL of a solution containing of 1.41 g (12.3 mmol) of octane, 0.13 g (1.18 mmol) of 1-octene, 0.015 g (0.11 mmol) of ethyl benzene hydroperoxide (EBHP), 0.036 g (0.32 mmol) of ethyl benzene, and 0.0129 g (0.10 mmol) of n-nonane as an internal standard. Sample aliquots were collected after 10 min, 30 min, and 60 min. Sampling involved removing approximately 0.4 mL of solution and filtering the solution through a 0.2 μm syringe filter. The samples were analyzed using a gas chromatograph (Agilent 6890, HP-1 methylsilicone capillary column, FID detector).

Micro-Scale Batch Reaction

0.050 g of catalyst was dried in the presence of molecular sieve (4 Å) in a 100 mL round-bottom flask at 120°C for 1 h under vacuum. The flask was then cooled to 70°C, purged with argon, and filled with 20 mL of a solution containing 14.02 g (123 mmol) of octane, 1.32 g

(11.7 mmol) of 1-octene, and 0.12 g (0.94 mmol) of n-nonane as an internal standard. After heating the solution to 70°C, the reaction was started by adding a solution containing 0.17 g (1.2 mmol) of EBHP and 0.34 g (3.17 mmol) of ethyl benzene. Sample aliquots were collected at 10 s, 1 min, 2 min, 5 min, 10 min, 30 min, and 60 min. The 10 s aliquot was considered as a 0% conversion datum. Sampling involved removing approximately 0.4 mL of solution and filtering the solution through a 0.2 μm syringe filter. The materials were analyzed using a gas chromatograph (Agilent 6890, HP-1 methylsilicone capillary column, FID detector).

Olefin epoxidation catalysis in a flow reactor

Zeotype catalysts were pelletized to a particle size of 180-250 μm. Approximately 0.1 g of catalyst was packed into a stainless-steel reactor (l = 41 mm, ∅ = 6 mm) between layers of glass wool. Layers of glass beads before and after the catalyst layer were used to stabilize the catalyst bed in the middle of the reactor and enable thorough mixing of the reaction solution. The reaction solution consisted of 80.6 g (720 mmol) of 1-octene, 9.54 g (62.7 mmol) of cumene hydroperoxide (cumene HP), and 7.4 g (64.8 mmol) of octane as an internal standard. The packed reactor was heated under vacuum at 120°C for 16 h. After cooling to room temperature, the reactor was flushed with octane and connected to a syringe that contained the reaction solution. The flow rate was controlled using a syringe pump. The reactor was placed in an oven at 45°C. The flow was started at a rate of 3 mL/h and was decreased to 0.3 mL/h after two hours. The temperature of the reactor was step-wise increased in ~10 K increments, until the EBHP conversion exceeded 90%. In order to allow the system to equilibrate, material collection started at least 1 h after the experiments were started. EBHP conversion of initial samples (less than 10 h time on stream) was determined via iodometric titration and subsequent samples were analyzed by gas chromatography (Agilent 6890, HP-1 methylsilicone capillary column, FID detector).

Results and Discussion

A series of B-SSZ-70 zeotypes was synthesized with varying CTAOH content in the synthesis gel, by substituting the conventional organic structure directing agent (OSDA) diisobutylimidazolium hydroxide (DIBI) with organic base CTAOH ($n_{CTAOH}/n_{(CTAOH + OSDA)}$) =

between 0 mol% and 100 mol% – see Table S1, Supporting Information). In the following sections of this manuscript, materials are labeled with regard to the degree of OSDA substitution with CTAOH, e.g., a material referred to as "19 mol% CTAOH" was synthesized by substituting 19 mol% of the OSDA with CTAOH in the synthesis gel.

Powder X-ray diffraction

Powder X-ray diffraction (PXRD) data in Figure 3a characterize the crystallinity and structural integrity of the as-synthesized materials. All materials exhibit well-defined peaks at 7.1°, 19.5°, 22.2°, and 26.1° 2θ, which are characteristic of the B-SSZ-70(P) structure (reference material labeled '0 mol% CTAOH' in Figure 3a), except for the ones synthesized with the two-highest CTAOH amounts, corresponding to 91 mol% and 100 mol% CTAOH. We surmise that all of these materials with the exception of the 91 and 100 mol% CTAOH are crystalline and structurally resemble as-synthesized B-SSZ-70(P). While even the 100 mol% CTAOH material exhibits characteristic peaks for B-SSZ-70(P), their intensities are weak, and the PXRD pattern of this material is identical to a physical mixture of amorphous silica and B-SSZ-70(P) seed crystals (at the same mass percentage as added to the zeotype synthesis gel). We conclude that in this high-CTAOH concentration hydrothermal synthesis, no additional crystalline phase forms. For the 91 mol% CTAOH material, we observe greater intensity of nearly all characteristic peaks in Figure 3a compared to the 100 mol% CTAOH material, implying that some crystalline material has been synthesized during hydrothermal treatment. This arises presumably as a consequence of the small amount (9 mol%) of OSDA in the synthesis gel, though based on its lower overall characteristic-peak intensity compared to other materials with lower CTAOH amounts, we hypothesize there is also amorphous material synthesized in the 91 mol% CTAOH material. To confirm this, we performed low-angle PXRD, and results are shown in Figure 3b. We observe a low-angle peak at 1.8° in the 91 mol% CTAOH material. This is known to represent mesoporous silica templated by CTA^+ as a surfactant.[47] We therefore conclude that the 91 mol% CTAOH material consists of some mesoporous amorphous silica.

Materials synthesized with between 53 mol% and 91 mol% CTAOH show a gradual disappearance of the 002 peak at 6.42°, and the growth of a peak at 5.6° (5.1° for the 91 mol% CTAOH material), which can be assigned to 003 of a new, swollen structure shown in Figure 3b,

as CTAOH content increases.[48] This is a consequence of a swollen zeotype layer phase, representing CTA^+ intercalation between zeotype layers. We calculate an increased interlayer distance from 2.5 Å to 22.3 Å based on the disappearance of the 002 peak of the non-swollen structure and appearance of the 003 peak of the swollen structure (see Figure S8 in Supporting Information for details). We conclude based on these data that the 53 mol% CTAOH material is partially swollen, in the sense of consisting of a mixture of swollen and non-swollen phases, and that the 77 mol% CTAOH material is fully swollen.[49] The latter is schematically represented in Figure 2. Similar swelling of layers has been previously reported in the Al-SSZ-70 layered-zeolite precursor.[45] The same materials that show the growth of the 003 peak at 5.6° 2θ (53 mol% and 77 mol% CTAOH materials; this new peak is observed at 5.1° 2θ instead in the 91 mol% CTAOH material) also show broadening and eventual fusion of the two peaks at 7.6° and 9.2°. Such a broadening and fusion has been previously identified to be a consequence of structural disorder between zeotype layers in both SSZ-70 and MWW zeotypes, and is an expected consequence of CTAOH chains intercalating between zeotype layers.[50] Such swelling was not reported previously when adding CTAB to MWW aluminosilicate synthesis with hexamethyleneimine (HMI) as OSDA,[42] but it has been observed in other MWW-related syntheses containing CTAB with a cationic imidazolium OSDA, including Ti-B-silicates.[12] We note in passing that the transition to amorphous products occurred at much lower amounts of CTAB in the former example employing neutral HMI[42] versus the latter cationic imidazolium OSDA.[12] It also occurred at much lower amounts of CTAB compared to our results here. We interpret this to be a consequence of the cationic imidazolium rather than neutral OSDA, with the former having stronger interactions with the framework.

Materials synthesized with less than 53 mol% CTAOH in the synthesis gel exhibit a broadening rather than gradual disappearance of the 002 peak at 6.42° 2θ (Figure 3c) upon increasing CTAOH content, and do not exhibit any growth of a new 003 peak of a swollen structure. This peak broadening begins to be evident in the material synthesized with 4 mol% CTAOH (FWHM = 0.29° for 4 mol% CTAOH material, vs. 0.36° for 10 mol% CTAOH material, vs. 0.44° for 19 mol% CTAOH material) in Figure 3c. Between 19 – 22 mol% CTAOH, the observed broadening of the 002 peak plateaus. This broadening behavior is in stark contrast to observations with MWW aluminosilicates using HMI as the OSDA and to which CTAB is added directly to the

synthesis gel. In those materials, no broadening of the 002 peak from the PXRD pattern was reported upon CTAB addition – only disappearance of this peak.[42]

We ascribe the broadening of the 002 peak, which corresponds to the stacking direction of the SSZ-70 layers, to be a consequence of decreasing crystallite thickness. We hypothesize that as the CTAOH content in the synthesis gel increases from 4 – 22 mol% CTAOH, crystal growth is limited along the z-axis, consequently leading to crystallites comprising fewer layers and thinner stacks. Similar roles of CTAOH limiting crystal growth have been noted previously for MFI synthesis.[40] Thus, CTAOH plays a dual role in our system, in terms of it acting both to swell (which has been extensively discussed previously[12,51,52] – a conventional role for CTAOH for layered zeolite precursors such as B-SSZ-70(P)) as well as to limit crystallite thickness in the c-direction. This dual function is summarized in Figure 2. Further support for this dual role is provided by the two characteristic CTAOH environments detected by ^{13}C solid-state NMR spectroscopy below.

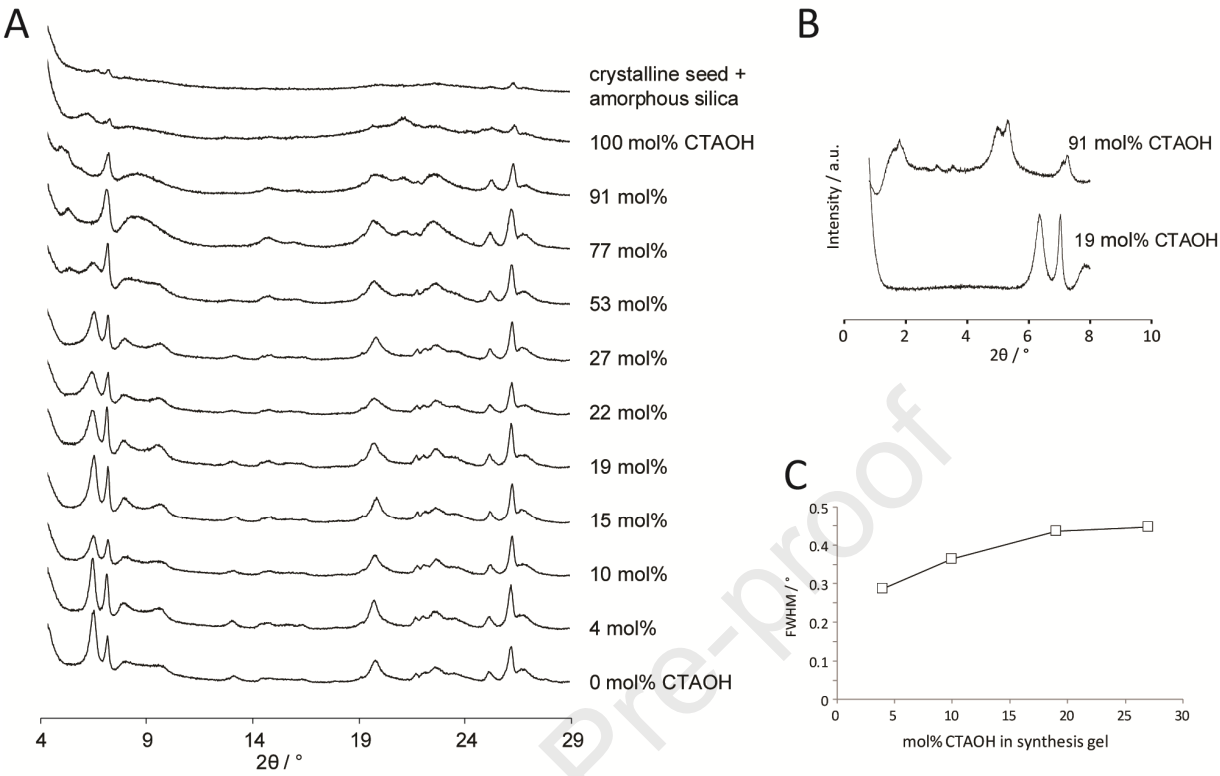

Figure 3. (A) PXRD patterns of as-synthesized materials synthesized with varying amounts of CTAOH in the synthesis gel. CTAOH contents are reported in mol% CTAOH. The inset in (B) shows the low-angle PXRD pattern for representative materials. (C) FWHM of the powder X-ray diffraction peak 002 as a function of mol% CTAOH in the synthesis gel for as-synthesized materials.

Elemental Analysis

Results from elemental (CHN) analysis were used to determine organic content of as-synthesized materials (after removal of excess synthesis solution following water wash). According to data in Figure 4, we identified three distinct regimes (I-III) of materials synthesis, depending on the CTAOH content in the synthesis gel. Regime I corresponds to materials synthesized between 0 – 27 mol% CTAOH in the synthesis gel. In this regime, CTA^+ content in as-synthesized materials following a brief wash is proportional to CTAOH amount in the synthesis gel, up to 0.1 g CTA^+ per g of zeotype product (corresponding to the 27 mol% CTAOH material). In this regime, we observe slightly decreasing OSDA content in the as-synthesized materials with varying CTAOH content in the synthesis gel, starting at 0.18 g per g product. This OSDA content agrees well with

several previously reported SSZ-70 materials, including B-SSZ-70.[53] In regime II, when increasing the CTAOH content in the synthesis gel further, OSDA remains unchanged, and the CTA^+ content plateaus. Only when exceeding a certain threshold of CTAOH content in the synthesis gel corresponding to the 77 mol% CTAOH material, an abrupt decrease of OSDA content and a rapid increase of CTA^+ is observed, which defines regime III.

Correlating CHN analysis and PXRD data shows that regime-I materials also exhibit a systematic broadening of the 002 peak in Figure 3. As discussed above, a broader 002 peak corresponds to the synthesis of thinner B-SSZ-70 crystallites, a phenomenon that we hypothesize is facilitated by CTA^+ bonding to the external surface, thereby lowering surface energy. We ascribe the hallmark of regime I, proportional increase of CTA^+ content upon increasing CTAOH concentration in the synthesis gel, to reflect the need to supply CTA^+ for this external-surface assembly while zeolite crystallite thickness decreases (i.e. more external surface is being synthesized upon increasing CTA^+ levels in regime I). Based on the only slightly decreasing OSDA content in Figure 4 and the uniform crystallinity in Figure 3 observed for materials in regime I, we surmise that the interior micropores of the zeolite crystallite are occupied with OSDA rather than CTA^+. Based on data in Figure 3b for the 19 mol% CTAOH material – taken as a representative material from regime I – we observe an absence of low-angle peaks in the PXRD pattern. We conclude that the 19 mol% CTAOH material lacks mesoporous amorphous silica and does not undergo swelling.[47]

PXRD data of the two materials that were synthesized in regime II exhibit swelling of the zeotype layers (by the appearance of a 003 reflection), which was not observed for materials in regime I, as well as disappearance of the 002 peak. In the swollen material, individual zeotype nanosheets assemble along the z axis, and CTA^+ cations are now located in a swollen environment, to be contrasted with regime I where they were located on the external surfaces of crystallites, as shown in Figure 2. This more ordered assembly of individual zeotype nanosheets is similar to those used to synthesize previously reported liquid-crystalline assemblies involving oligomeric silica colloids and CTA^+ in solution,[27,28] and such assemblies appear to require higher CTA^+ amounts added to the synthesis gel, marked by regime II. We summarize that both of the regime-II materials synthesized with 53 mol% and 77 mol% CTAOH in the synthesis gel

are partially and fully swollen, respectively, and have a higher CTA^+ content in Figure 4 (0.15 and 0.12 g CTA^+ per g material, respectively) compared with the material synthesized with 27 mol% CTAOH, which is not swollen and contains 0.10 g CTA^+ per g material. Low angle PXRD data confirms absence of peaks at 1.8° 2θ in the 77 mol% CTAOH material (see Figure S13, Supporting Information), so we conclude that regime-II materials lack a mesoporous amorphous silica phase.

In regime III, which comprises materials synthesized with a CTAOH content of > 77 mol% in the synthesis gel, a steep increase of CTA^+ content is observed as well as a decreasing OSDA content, with increased CTAOH content in the synthesis gel. According to PXRD data, these materials are partially amorphous. We surmise that the observed synthesis of amorphous silica in these materials is influenced by CTAOH, which accounts for the higher CTA^+ content in these latter two materials.

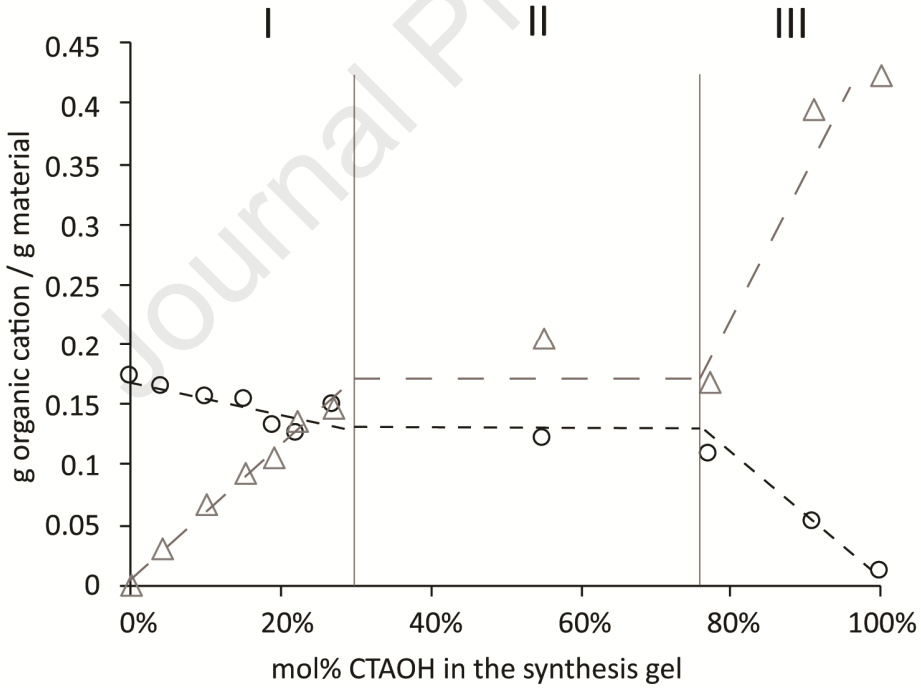

Figure 4. Dependency of CTA^+ (Δ) and $OSDA^+$ comprising DIBI (○) content in the as-synthesized materials on the amount of CTAOH in the synthesis gel. Dashed lines are drawn as a guide to the eye.

^{13}C NMR spectroscopy

We used ^{13}C MAS NMR spectroscopy in order to characterize the molecular environment surrounding CTA^+ cations in the as-synthesized materials. We chose two materials that represent regimes I and II in Figure 4, which were synthesized with 19 mol% (CTA^+ cations terminate the external surface of the crystallite and limit its growth) and 77 mol% (swollen by CTA^+ cations) CTAOH in the synthesis gel. Bloch-decay ^{13}C NMR spectra of these two materials are shown in Figure 5. A reference spectrum of the neat (crystalline) OSDA (DIBI) is shown below the spectra of the materials. All resonances were assigned to either CTA^+ or $OSDA^+$, and are consistent with prior literature assignments.[54] The 19 mol% CTAOH material exhibits narrow resonances for CTA^+, and broad ones for OSDA in Figure 5. This suggests mobile CTA^+ and immobile OSDA in this material, based on a previously reported correlation between NMR peak width and surfactant mobility.[55]

As mentioned above on the basis of PXRD data, we expect DIBI OSDA to reside in the confining zeotype micropores, where mobility is most restricted. CTA^+ mobility in the 19 mol% CTAOH material is further supported by CP-MAS (0.1 ms for contact time) ^{13}C NMR spectra (see Figure S6, Supporting Information), where CTA^+ resonances are not detected that are otherwise observable in the MAS ^{13}C NMR spectrum of Figure 5. This is due to CTA^+ mobility and consequent lack of C-H dipolar coupling for efficient cross-polarization buildup. These data are qualitatively consistent with the proposed environment for CTA^+ in the 19 mol% CTAOH material, based on the role of CTA^+ terminating the zeotype-crystallite external surface as schematically represented for this material in Figure 2, where the tails of the CTA^+ molecules are unrestricted in their mobility. We assign this type of environment to be similar to that previously observed initially (following two days of crystallization) by solid-state NMR spectroscopy of MFI synthesized by employing CTAOH as OSDA.[40] In this prior report, this CTA^+ environment also corresponded to a highly mobile state, in which no resonance for the methyl tail of CTA^+ was observed via CP-MAS ^{13}C NMR spectroscopy. This was supported with 2D ^{1}H-^{29}Si HETCOR MAS NMR spectroscopic data, which demonstrated that while there was proximity between the charged headgroup of CTA^+ and the siliceous surface, there was no such proximity involving the adjacent methylenes attached to this headgroup. Based on these data, it was concluded that the hydrophobic tail of CTA^+ limited MFI crystal growth in this external-surface assembly.[40]

The ^{13}C MAS NMR spectrum of the 77 mol% CTAOH material exhibits two sets of resonances: (i) one that is identical with the assignment of carbon atoms of the C_{16} chain of CTA^+ and OSDA in the 19 mol% CTAOH material above, and (ii) another that represents a set of new, broad resonances, which appear systematically low-field shifted, close to resonances that were assigned to the mobile CTA^+ in (i). These new CTA^+ resonances are labeled C4 – C16 (im) in Figure 5 (see Figure S7, Supporting Information for overlaid spectra), and they can be observed as strong signals in the CP-MAS ^{13}C NMR spectrum with a short cross-polarization contact time of 0.1 ms (see Figure S6, Supporting Information). Since, according to PXRD data in Figure 3, the material synthesized with 77 mol% CTAOH is swollen, we surmise that these new peaks belong to CTA^+ that is distinctly located between two external surfaces of adjacent zeotype crystallites, as shown schematically in Figure 2. This environment results in less mobile CTA^+ compared to the one observed for the 19 mol% CTAOH material.

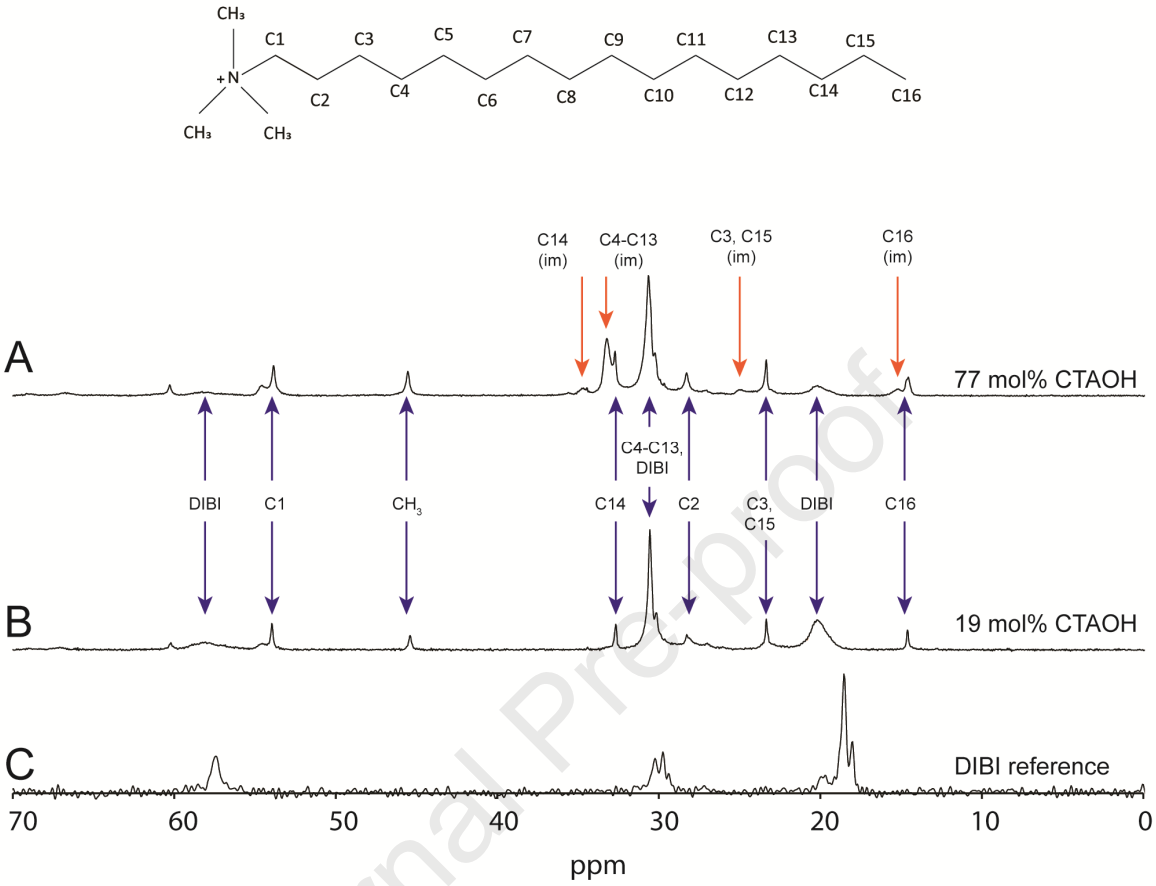

Figure 5. ^{13}C MAS NMR spectra of materials synthesized with (a) 77 mol% CTAOH and (b) 19 mol% CTAOH in the synthesis gel, and (c) a reference spectrum of the OSDA disobutyl imidazolium hydroxide (DIBI). For the CTA^+ cation in the 77 mol% CTAOH material, assignments in orange with the note "(im)" are assigned to CTA^+ in an immobile environment.

Delamination

To investigate the correlation between ease of zeotype delamination and crystallite thickness, we treated the as-synthesized materials in a high-shear mixer (see Experimental for details on procedure). Our rationale for using high-shear mixing was to affect mechanical agitation in a way that could replace the ubiquitous need for sonication, which has often been a workhorse for achieving delamination in the past (sonication is difficult to scale).

To rapidly assess the effect of high-shear mixing on delamination in all as-synthesized materials, we used a combination of N_2 physisorption, titanium elemental analysis, and catalysis. N_2 physisorption was performed on materials that were calcined after high-shear mixing. Titanium elemental analysis and catalysis were performed on samples that were calcined after high-shear mixing and exchanged with titanium for boron (see experimental and SI for details). Our rational here is that Ti content has been previously shown to be a direct reporter of external zeotype surface area,[20,23] and the bulky organic hydroperoxide substrate is known to productively bind during catalysis only at the external surface of the Ti-functionalized zeotype;[19] therefore, the titanium content as well as the observed catalytic activity directly reflects the external surface area available for a particular catalyst.[20,23]

Figure 6 shows the Ti content of delaminated zeotype catalysts plotted as a function of CTAOH content in the zeotype synthesis gel. Materials with high Ti contents (167 μmol Ti g^{-1} [Si:Ti = 100] and 329 μmol Ti g^{-1} [Si:Ti = 51]) are the ones synthesized with 91 mol% and 100 mol% CTAOH in the synthesis gel, respectively. This can be explained by their partial amorphous character, which synthesizes a high external surface area support for Ti grafting. Measurements of the external surface area of these two materials preceding Ti incorporation (i.e. after first calcination) via N_2 physisorption are summarized in Table 1, and show them to be the highest of all materials investigated – representative of mesoporous amorphous silica with nearly no microporosity. This lack of microporosity in the amorphous silica synthesized in regime III of Figure 4 is consistent with prior reports of synthesizing amorphous silica when using too high an amount of CTA^+ in the zeotype synthesis gel.[42]

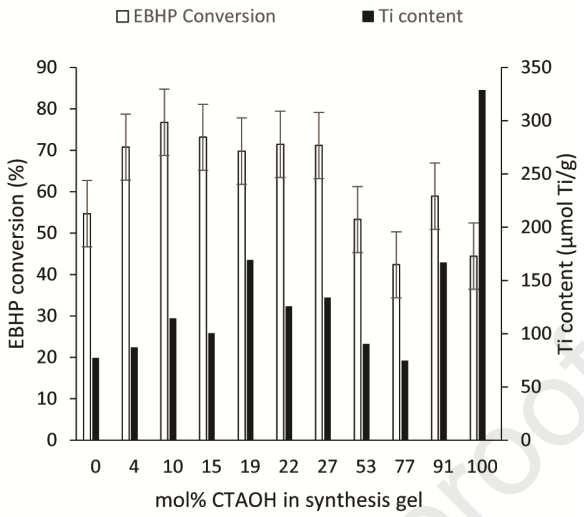

Figure 6. Ti-content and conversion of EBHP during small-scale batch epoxidation of 1-octene at 70°C for high-shear mixed and calcined materials as a function of mol% CTAOH in the synthesis gel. Conversion of EBHP was measured at 60 min and the reaction mixture consisted of 0.005 g high-shear-mixed material as catalyst, 1.41 g of octane, 0.13 g of 1-octene, 0.015 g of EBHP, 0.036 g of ethyl benzene, and 0.0129 g n-nonane.

Crystalline catalysts based on materials from regime I in Figure 4 (in which the hypothesized function of CTA^+ is to terminate the external surface of the crystallites, as shown in Figure 2) span materials that were synthesized with between 0 mol% CTAOH and 27 mol% CTAOH in the synthesis gel. These catalysts generally exhibit an increasing Ti content from about 75 μmol g^{-1} (Si:Ti = 222) for the catalyst derived from the 0 mol% CTAOH material to about 120 μmol g^{-1} (Si:Ti = 139) for the catalyst derived from the 27 mol% CTAOH material. The exception is the catalyst derived from the 19 mol% CTAOH material, which exhibits a local Ti-content maximum of 169 μmol Ti/g [Si:Ti = 99]. The latter material is referred to as **Ti-1**, and the precursor to this material prior to Ti incorporation (i.e. after first calcination) is referred to as **1**. N_2 physisorption data in Table 1 demonstrate **1** to have a 1.6-fold higher external surface area (109 m^2/g) than the 0% CTAOH material (67 m^2/g). In contrast, crystalline materials with 51 mol% and 77 mol% CTAOH in the synthesis gel, where CTA^+ acts as a swelling agent, as shown in Figure 2, exhibit the lowest Ti content of the series (91 μmol Ti g^{-1} [Si:Ti = 183] and

75 μmol Ti g^{-1} [Si:Ti = 222], respectively), which is consistent with their low (69 m^2/g for the material made with 77 mol% CTAOH) external surface area, as measured by N_2 physisorption.

The data above are consistent with the measured catalytic activity of the materials shown in Figure 6, using a batch screening reaction involving 1-octene and ethylbenzene hydroperoxide (EBHP) as organic oxidant. The data demonstrate that high-shear-mixed materials synthesized with between 4 mol% and 27 mol% CTAOH show the highest catalytic activities of all materials (average EBHP conversion > 65%) and show a significantly higher catalytic activity of up to 1.4-times higher EBHP conversion (19 mol% CTAOH material) than the material prepared with 0% CTAOH in the synthesis gel (EBHP conversion 55%). In contrast, catalysts based on materials with 53 mol% CTAOH and 77 mol% CTAOH exhibit an average EBHP conversion of 48%, which is only slightly lower than the partial amorphous materials comprising 91 mol% and 100 mol% CTAOH in the synthesis gel (average EBHP conversion = 52%) and nearly the same as that of the catalyst synthesized from the 0 mol% CTAOH material. These trends parallel external surface area measurements and Ti content of the catalysts. The low activity of the partial amorphous materials (despite its higher titanium content) is consistent with literature data, which demonstrated the inferior catalytic performance of amorphous titanosilica materials despite their higher external surface area and higher titanium content when compared to crystalline materials.[22] This is a consequence of more favorable entropies of activation when catalysis is conducted in pockets on the zeolite external surface.[56,57]Presumably for the same reason, the partially amorphous material synthesized with 91 mol% CTAOH exhibits a higher activity than the nearly completely amorphous material synthesized with 100 mol% CTAOH.

To investigate the importance of high-shear mixing for delamination, we synthesized a control material that was not high-shear mixed but otherwise followed the same synthesis as **1**. This zeotype support **2** had lower external surface area compared with **1.** (S_{ext}(**2**) = 80 m^2/g vs S_{ext}(**1**) = 109 m^2/g; see Table 1). To address, whether these observed differences are due to delamination versus any decrease in crystallite size after high-shear mixing, we imaged **1** and **2** (see Figure S14, Supporting Information). These images demonstrate similar crystallite sizes for **1** and **2**. Altogether, these data demonstrate the importance of high-shear mixing on achieving a material with greater delamination. After Ti-incorporation to both of these supports, we synthesized

catalysts **Ti-1** (based on **1**) and **Ti-2** (based on **2**). **Ti-2** exhibits a lower catalytic activity (40% EBHP conversion) compared to **Ti-1** (69% EBHP conversion; see Figure S5, Supporting Information) in a batch olefin epoxidation reaction, which was performed identically to the procedure described in Figure 6. This higher activity for Ti-1 is expected on the basis that **1** has a higher surface area, since our probe reaction can only occur on the external surface due to the sterically bulky reactants involved. These results further support the importance of high-shear mixing on the synthesis of delaminated zeotype catalysts.

In summary, based on the physisorption data, elemental analyses, and catalysis data above, we surmise (i) that the presence of CTA^+ as a capping group that limits crystallite thickness of the B-SSZ-70 precursor (e.g., in the 19 mol% CTAOH material) facilitates delamination via high-shear mixing and (ii) that the presence of CTA^+ as a swelling agent (e.g., in the 77 mol% CTAOH material) in the layered zeolite precursor correlates negatively with ease of delamination. Our data are in stark contrast to the commonly held conventional view of swelling being a required prerequisite intermediate in the kinetic pathway that connects a layered-zeolite-precursor starting material and a delaminated-zeotype final product.[15,44,48] This view maintains swelling as a process that facilitates delamination by beginning to peel layers apart from each other in the precursor material. We rationalize these conflicting perspectives by viewing swelling in our system as a phenomenon that organizes individual zeotype nanosheets into an ordered assembly (see solid-state NMR results above) along the crystallographic z axis, which are predisposed to condense upon calcination (i.e. regime II in Figure 4 and represented schematically in Figure 2), compared to the isolated crystallites of regime I – which lead to higher Ti contents (and inferred external surface areas) for catalysts. From the perspective of achieving a high external surface area after delamination, we conclude that swelling is counterproductive in our system, as it pre-organizes the system towards a three-dimensional rather than two-dimensional zeolite upon calcination. This preorganization is unable to be broken by the mild high-shear mixing approach that is used here to affect delamination. Said another way, it is easier for high-shear mixing to keep the isolated crystallite external surfaces of regime I apart as well as to separate layers from these crystallites, which are held together by $OSDA^+$, than it is to isolate individual nanosheets from a preorganized swollen structure in regime II,

which are held together by CTA^+. The latter requires harsher mechanical treatment such as ultrasonication in order to separate the nanosheets.[18]

Table 1. Textural properties of selected materials

Material	S_{ext} (m^2/g)	S_{tot} (m^2/g)	V_{mic} (cm^3/g)	V_{tot} (cm^3/g)
100 mol% CTAOH	396	380	0	0.47
91 mol% CTAOH	132	388	0.11	0.45
77 mol% CTAOH	69	299	0.09	0.28
19 mol% CTAOH Material **1**	109	549	0.18	0.34
19 mol% CTAOH not high-shear-mixed (Material **2**)	80	503	0.17	0.29
0 mol% CTAOH	67	438	0.15	0.29
UCB-4	100	479	0.15	0.34

Conclusions

We investigated the substitution of $OSDA^+OH^-$ with CTA^+OH^- in the B-SSZ-70 zeotype synthesis gel from the perspective of (i) limiting the crystal size for as-synthesized zeotype, and (ii) impacting delamination using high-shear mixing, without the need for sonication and halide reagents used in conventional SSZ-70 delamination approaches. Our results demonstrate three distinct regimes depending on the degree of substitution: (I) at low CTA^+ levels (< 50 mol% as a fraction of total organic base in the zeotype synthesis gel), we observed CTA^+ terminating the zeotype external surface and the formation of thinner crystallites; (II) at substitution levels between 55 and 75 mol%, our data indicates that CTA^+ intercalates between individual zeotype layers, which leads to zeotype layer swelling; and (iii) at substitution levels above 90 mol%, the formation of mostly amorphous silica was observed. After delaminating the as-synthesized materials with high-shear mixing and synthesizing catalysts via isomorphous substitution of B with Ti, catalysts based on materials synthesized in regime (I) above exhibit higher Ti loadings and enhanced catalytic performance – both metrics that scale with external surface area –

compared with swollen materials synthesized in regime (II) above. These data lead us to conclude that swelling *per se* is not directly correlated with ease of delamination; instead, in our system, it is the thinner crystallite size that facilitates delamination. This small size is brought about by bonding of CTA^+ to the external surface, which lowers the surface energy. Altogether, our data here support a new mild synthetic approach for SSZ-70 delamination and emphasize the lack of prerequisite for swelling in this approach. The grafted Ti-containing olefin epoxidation catalysts synthesized using the delaminated materials showed a 1.4-fold higher hydroperoxide conversion compared with the non-delaminated zeotype.

Acknowledgements

The authors gratefully acknowledge funding from the National Science Foundation Small Business Innovation Research Program (NSF-SBIR, Award No. 1746827) for materials synthesis and funding from the U.S. Department of Energy (DE-FG02-05ER15696) for materials characterization.

Conflicts of interest

There are no conflicts of interest to declare.

References

[1] N.A. Grosso-Giordano, S.I. Zones, A. Katz, Opportunities for controlling catalysis by designing molecular environments around active sites: cations supported on amorphous versus crystalline zeolitic silicate supports, in: Catal. Vol. 31, 2019: pp. 72–126. https://doi.org/10.1039/9781788016971-00072.

[2] T.F. Degnan, C.M. Smith, C.R. Venkat, Alkylation of aromatics with ethylene and propylene: recent developments in commercial processes, Appl. Catal. A Gen. 221 (2001) 283–294. https://doi.org/10.1016/S0926-860X(01)00807-9.

[3] K.-G. Haw, J.-P. Gilson, N. Nesterenko, M. Akouche, H. El Siblani, J.-M. Goupil, B.

Rigaud, D. Minoux, J.-P. Dath, V. Valtchev, Supported Embryonic Zeolites and their Use to Process Bulky Molecules, ACS Catal. 8 (2018) 8199–8212. https://doi.org/10.1021/acscatal.8b01936.

[4] Z. Qin, L. Pinard, M.A. Benghalem, T.J. Daou, G. Melinte, O. Ersen, S. Asahina, J.-P. Gilson, V. Valtchev, Preparation of Single-Crystal "House-of-Cards"-like ZSM-5 and Their Performance in Ethanol-to-Hydrocarbon Conversion, Chem. Mater. 31 (2019) 4639–4648. https://doi.org/10.1021/acs.chemmater.8b04970.

[5] S. Mintova, J.-P. Gilson, V. Valtchev, Advances in nanosized zeolites, Nanoscale. 5 (2013) 6693. https://doi.org/10.1039/c3nr01629c.

[6] W.-S. Ahn, R. Ryoo, C. Jo, K. Na, J. Kim, MFI Titanosilicate Nanosheets with Single-Unit-Cell Thickness as an Oxidation Catalyst Using Peroxides, ACS Catal. 1 (2011) 901–907. https://doi.org/10.1021/cs2002143.

[7] J. Jung, C. Jo, K. Cho, R. Ryoo, Zeolite nanosheet of a single-pore thickness generated by a zeolite-structure-directing surfactant, J. Mater. Chem. 22 (2012) 4637. https://doi.org/10.1039/c2jm16539b.

[8] N.D. Hould, S. Kumar, M. Tsapatsis, V. Nikolakis, R.F. Lobo, Structure and colloidal stability of nanosized zeolite beta precursors, Langmuir. 26 (2010) 1260–1270. https://doi.org/10.1021/la902445c.

[9] C. Anand, Y. Yamaguchi, Z. Liu, S. Ibe, S.P. Elangovan, T. Ishii, T. Ishikawa, A. Endo, T. Okubo, T. Wakihara, Pioneering In Situ Recrystallization during Bead Milling: A Top-down Approach to Prepare Zeolite A Nanocrystals, Sci. Rep. 6 (2016) 29210. https://doi.org/10.1038/srep29210.

[10] J. Jiang, J. Yu, A. Corma, Extra-large-pore zeolites: bridging the gap between micro and mesoporous structures, Angew. Chemie - Int. Ed. 49 (2010) 3120–3145. https://doi.org/10.1002/anie.200904016.

[11] X. Ji, L. Xu, X. Du, X. Lu, W. Lu, J. Sun, P. Wu, Simple CTAB surfactant-assisted hierarchical lamellar MWW titanosilicate: A high-performance catalyst for selective oxidations involving bulky substrates, Catal. Sci. Technol. 7 (2017) 2874–2885. https://doi.org/10.1039/c7cy00756f.

[12] L. Xu, X. Ji, S. Li, Z. Zhou, X. Du, J. Sun, F. Deng, S. Che, P. Wu, Self-Assembly of Cetyltrimethylammonium Bromide and Lamellar Zeolite Precursor for the Preparation of

Hierarchical MWW Zeolite, Chem. Mater. 28 (2016) 4512–4521. https://doi.org/10.1021/acs.chemmater.6b02155.

[13] W.J. Roth, J. Čejka, Two-dimensional zeolites: dream or reality?, Catal. Sci. Technol. 1 (2011) 43. https://doi.org/10.1039/c0cy00027b.

[14] H.Y. Luo, V.K. Michaelis, S. Hodges, R.G. Griffin, Y. Román-Leshkov, One-pot synthesis of MWW zeolite nanosheets using a rationally designed organic structure-directing agent, Chem. Sci. 6 (2015) 6320–6324. https://doi.org/10.1039/C5SC01912E.

[15] S. Maheshwari, E. Jordan, S. Kumar, F.S. Bates, R.L. Penn, D.F. Shantz, M. Tsapatsis, Layer Structure Preservation during Swelling, Pillaring, and Exfoliation of a Zeolite Precursor, J. Am. Chem. Soc. 130 (2008) 1507–1516. https://doi.org/10.1021/ja077711i.

[16] U. Díaz, A. Corma, Layered zeolitic materials: An approach to designing versatile functional solids, Dalt. Trans. 43 (2014) 10292–10316. https://doi.org/10.1039/c3dt53181c.

[17] A. Corma, V. Fornés, J.. Guil, S. Pergher, T.L.. Maesen, J.. Buglass, Preparation, characterisation and catalytic activity of ITQ-2, a delaminated zeolite, Microporous Mesoporous Mater. 38 (2000) 301–309. https://doi.org/10.1016/S1387-1811(00)00149-9.

[18] I. Ogino, E.A. Eilertsen, S.J. Hwang, T. Rea, D. Xie, X. Ouyang, S.I. Zones, A. Katz, Heteroatom-tolerant delamination of layered zeolite precursor materials, Chem. Mater. 25 (2013) 1502–1509. https://doi.org/10.1021/cm3032785.

[19] X. Ouyang, Y.-J. Wanglee, S.-J. Hwang, D. Xie, T. Rea, S.I. Zones, A. Katz, Novel surfactant-free route to delaminated all-silica and titanosilicate zeolites derived from a layered borosilicate MWW precursor., Dalton Trans. 43 (2014) 10417–29. https://doi.org/10.1039/c4dt00383g.

[20] A. Okrut, M. Aigner, C. Schöttle, N.A. Grosso-Giordano, S.J. Hwang, X. Ouyang, S. Zones, A. Katz, SSZ-70 borosilicate delamination without sonication: effect of framework topology on olefin epoxidation catalysis, Dalt. Trans. 47 (2018) 15082–15090. https://doi.org/10.1039/C8DT03044H.

[21] X. Ouyang, S.J. Hwang, D. Xie, T. Rea, S.I. Zones, A. Katz, Heteroatom-substituted delaminated zeolites as solid lewis acid catalysts, ACS Catal. 5 (2015) 3108–3119. https://doi.org/10.1021/cs5020546.

[22] M. Aigner, N.A. Grosso-Giordano, C. Schöttle, A. Okrut, S. Zones, A. Katz, Epoxidation

of 1-octene under harsh tail-end conditions in a flow reactor II: impact of delaminated-zeolite catalyst surface area and structural integrity on catalytic performance, React. Chem. Eng. 2 (2017) 852–861. https://doi.org/10.1039/C7RE00138J.

[23] M. Aigner, N.A. Grosso-Giordano, A. Okrut, S. Zones, A. Katz, Epoxidation of 1-octene under harsh tail-end conditions in a flow reactor I: a comparative study of crystalline vs. amorphous catalysts, React. Chem. Eng. 2 (2017) 842–851. https://doi.org/10.1039/C7RE00076F.

[24] X. Ouyang, S.J. Hwang, R.C. Runnebaum, D. Xie, Y.J. Wanglee, T. Rea, S.I. Zones, A. Katz, Single-step delamination of a MWW borosilicate layered zeolite precursor under mild conditions without surfactant and sonication, J. Am. Chem. Soc. 136 (2014) 1449–1461. https://doi.org/10.1021/ja410141u.

[25] A. Okrut, N.A. Grosso-Giordano, C. Schöttle, S. Zones, A. Katz, Understanding the role of Zn 2+ in surfactant-free layered silicate delamination: Exfoliation of magadiite, Microporous Mesoporous Mater. 283 (2019) 55–63. https://doi.org/10.1016/j.micromeso.2019.03.048.

[26] E.A. Eilertsen, I. Ogino, S.J. Hwang, T. Rea, S. Yeh, S.I. Zones, A. Katz, Nonaqueous fluoride/chloride anion-promoted delamination of layered zeolite precursors: Synthesis and characterization of UCB-2, Chem. Mater. 23 (2011) 5404–5408. https://doi.org/10.1021/cm202364q.

[27] J.D. Epping, B.F. Chmelka, Nucleation and growth of zeolites and inorganic mesoporous solids: Molecular insights from magnetic resonance spectroscopy, Curr. Opin. Colloid Interface Sci. 11 (2006) 81–117. https://doi.org/10.1016/j.cocis.2005.12.002.

[28] Q. Huo, D.I. Margolese, U. Ciesla, D.G. Demuth, P. Feng, T.E. Gier, P. Sieger, A. Firouzi, B.F. Chmelka, Organization of Organic Molecules with Inorganic Molecular Species into Nanocomposite Biphase Arrays, Chem. Mater. 6 (1994) 1176–1191. https://doi.org/10.1021/cm00044a016.

[29] J. García-Martínez, M. Johnson, J. Valla, K. Li, J.Y. Ying, Mesostructured zeolite Y—high hydrothermal stability and superior FCC catalytic performance, Catal. Sci. Technol. 2 (2012) 987. https://doi.org/10.1039/c2cy00309k.

[30] I.I. Ivanova, E.E. Knyazeva, Micro–mesoporous materials obtained by zeoliterecrystallization: synthesis, characterization and catalytic applications, Chem. Soc.

Rev. 42 (2013) 3671–3688. https://doi.org/10.1039/C2CS35341E.

[31] J. Garcia-Martinez, C. Xiao, K.A. Cychosz, K. Li, W. Wan, X. Zou, M. Thommes, Evidence of intracrystalline mesostructured porosity in zeolites by advanced gas sorption, electron tomography and rotation electron diffraction, ChemCatChem. 6 (2014) 3110–3115. https://doi.org/10.1002/cctc.201402499.

[32] J. García-Martínez, K. Li, G. Krishnaiah, A mesostructured Y zeolite as a superior FCC catalyst – from lab to refinery, Chem. Commun. 48 (2012) 11841. https://doi.org/10.1039/c2cc35659g.

[33] T. Moteki, S.H. Keoh, T. Okubo, Synthesis of zeolites using highly amphiphilic cations as organic structure-directing agents by hydrothermal treatment of a dense silicate gel, Chem. Commun. 50 (2014) 1330–1333. https://doi.org/10.1039/C3CC48396G.

[34] D. Xu, J. Feng, S. Che, An insight into the role of the surfactant CTAB in the formation of microporous molecular sieves, Dalt. Trans. 43 (2014) 3612–3617. https://doi.org/10.1039/C3DT53308E.

[35] F. Hasan, R. Singh, G. Li, D. Zhao, P.A. Webley, Direct synthesis of hierarchical LTA zeolite via a low crystallization and growth rate technique in presence of cetyltrimethylammonium bromide, J. Colloid Interface Sci. 382 (2012) 1–12. https://doi.org/10.1016/j.jcis.2012.05.027.

[36] M. Kumar, H. Luo, Y. Román-Leshkov, J.D. Rimer, SSZ-13 Crystallization by Particle Attachment and Deterministic Pathways to Crystal Size Control, J. Am. Chem. Soc. 137 (2015) 13007–13017. https://doi.org/10.1021/jacs.5b07477.

[37] Y. Jin, Y. Li, S. Zhao, Z. Lv, Q. Wang, X. Liu, L. Wang, Synthesis of mesoporous MOR materials by varying temperature crystallizations and combining ternary organic templates, Microporous Mesoporous Mater. 147 (2012) 259–266. https://doi.org/10.1016/j.micromeso.2011.06.023.

[38] S.P. Naik, A.S.T. Chiang, R.W. Thompson, F.C. Huang, H.-M. Kao, Mesoporous silica with short-range MFI structure, Microporous Mesoporous Mater. 60 (2003) 213–224. https://doi.org/10.1016/S1387-18110300379-2.

[39] S. Hu, H. Jia, J. Ma, W. Hao, R. Li, A hierarchical zeolite microsphere prepared by an eco-friendly and practical route for efficient reaction of bulky molecules, Microporous Mesoporous Mater. 294 (2020) 109931.

https://doi.org/10.1016/j.micromeso.2019.109931.

[40] L. Meng, B. Mezari, M.G. Goesten, E.J.M. Hensen, One-Step Synthesis of Hierarchical ZSM-5 Using Cetyltrimethylammonium as Mesoporogen and Structure-Directing Agent, Chem. Mater. 29 (2017) 4091–4096. https://doi.org/10.1021/acs.chemmater.7b00913.

[41] A. Chawla, R. Li, R. Jain, R.J. Clark, J.G. Sutjianto, J.C. Palmer, J.D. Rimer, Cooperative effects of inorganic and organic structure-directing agents in ZSM-5 crystallization, Mol. Syst. Des. Eng. 3 (2018) 159–170. https://doi.org/10.1039/C7ME00097A.

[42] Y. Zhou, Y. Mu, M.-F. Hsieh, B. Kabius, C. Pacheco, C. Bator, R.M. Rioux, J.D. Rimer, Enhanced Surface Activity of MWW Zeolite Nanosheets Prepared via a One-Step Synthesis, J. Am. Chem. Soc. 142 (2020) 8211–8222. https://doi.org/10.1021/jacs.9b13596.

[43] S. Maheshwari, C. Martínez, M. Teresa Portilla, F.J. Llopis, A. Corma, M. Tsapatsis, Influence of layer structure preservation on the catalytic properties of the pillared zeolite MCM-36, J. Catal. 272 (2010) 298–308. https://doi.org/10.1016/j.jcat.2010.04.011.

[44] W.J. Roth, J. Čejka, R. Millini, E. Montanari, B. Gil, M. Kubu, Swelling and Interlayer Chemistry of Layered MWW Zeolites MCM-22 and MCM-56 with High Al Content, Chem. Mater. 27 (2015) 4620–4629. https://doi.org/10.1021/acs.chemmater.5b01030.

[45] R.C. Runnebaum, X. Ouyang, J.A. Edsinga, T. Rea, I. Arslan, S.J. Hwang, S.I. Zones, A. Katz, Role of delamination in zeolite-catalyzed aromatic alkylation: UCB-3 versus 3-D Al-SSZ-70, ACS Catal. 4 (2014) 2364–2368. https://doi.org/10.1021/cs500285w.

[46] A. Corma, V. Fornes, S.B. Pergher, T.L.M. Maesen, J.G. Buglass, Delaminated zeolite precursors as selective acidic catalysts, Nature. 396 (1998) 353–356. https://doi.org/10.1038/24592.

[47] A.J. Schwanke, C.W. Lopes, S.B.C. Pergher, Synthesis of Mesoporous Material from Chrysotile-Derived Silica, Mater. Sci. Appl. 04 (2013) 68–72. https://doi.org/10.4236/msa.2013.48A009.

[48] A.J. Schwanke, U. Díaz, A. Corma, S. Pergher, Recyclable swelling solutions for friendly preparation of pillared MWW-type zeolites, Microporous Mesoporous Mater. 253 (2017) 91–95. https://doi.org/10.1016/j.micromeso.2017.06.045.

[49] K. Lund, N. Muroyama, O. Terasaki, Accidental extinction in powder XRD intensity of porous crystals: Mesoporous carbon crystal CMK-5 and layered zeolite-nanosheets,

Microporous Mesoporous Mater. 128 (2010) 71–77. https://doi.org/10.1016/j.micromeso.2009.08.004.

[50] S. Smeets, Z.J. Berkson, D. Xie, S.I. Zones, W. Wan, X. Zou, M.-F.F. Hsieh, B.F. Chmelka, L.B. McCusker, C. Baerlocher, Well-Defined Silanols in the Structure of the Calcined High-Silica Zeolite SSZ-70: New Understanding of a Successful Catalytic Material, J. Am. Chem. Soc. 139 (2017) 16803–16812. https://doi.org/10.1021/jacs.7b08810.

[51] C.T. Kresge, W.J. Roth, Crysalline Oxide Material, 5,266,541, 1985. https://doi.org/10.1016/0375-6505(85)90011-2.

[52] A. Corma, V. Fornes, J. Martinez-Triguero, S.B. Pergher, Delaminated zeolites: Combining the benefits of zeolites and mesoporous materials for catalytic uses, J. Catal. 186 (1999) 57–63. https://doi.org/10.1006/jcat.1999.2503.

[53] R.H. Archer, J.R. Carpenter, S.-J. Hwang, A.W. Burton, C.-Y. Chen, S.I. Zones, M.E. Davis, Physicochemical Properties and Catalytic Behavior of the Molecular Sieve SSZ-70, Chem. Mater. 22 (2010) 2563–2572. https://doi.org/10.1021/cm9035677.

[54] (National Institute of Advanced Industrial Science and Technology, accessed on 6/18/2020), (n.d.). https://sdbs.db.aist.go.jp.

[55] K. Flodstrom, H. Wennerstrom, V. Alfredsson, Mechanism of Mesoporous Silica Formation . A Time-Resolved NMR and TEM Study of Silica - Block Copolymer Aggregation, Langmuir. (2004) 680–688. https://doi.org/10.1021/la030173c.

[56] N.A. Grosso-Giordano, A.S. Hoffman, A. Boubnov, D.W. Small, S.R. Bare, S.I. Zones, A. Katz, Dynamic Reorganization and Confinement of Ti IV Active Sites Controls Olefin Epoxidation Catalysis on Two-Dimensional Zeotypes, J. Am. Chem. Soc. 141 (2019) 7090–7106. https://doi.org/10.1021/jacs.9b02160.

[57] N.A. Grosso-Giordano, C. Schroeder, A. Okrut, A. Solovyov, C. Schöttle, W. Chassé, N. Marinković, H. Koller, S.I. Zones, A. Katz, Outer-Sphere Control of Catalysis on Surfaces: A Comparative Study of Ti(IV) Single-Sites Grafted on Amorphous versus Crystalline Silicates for Alkene Epoxidation, J. Am. Chem. Soc. (2018) jacs.7b11467. https://doi.org/10.1021/jacs.7b11467.

[58] I. Arslan, J.D. Roehling, I. Ogino, K.J. Batenburg, S.I. Zones, B.C. Gates, A. Katz, Genesis of Delaminated-Zeolite Morphology: 3-D Characterization of Changes by STEM

Tomography, J. Phys. Chem. Lett. 6 (2015) 2598–2602. https://doi.org/10.1021/acs.jpclett.5b01004.

Highlights:

In the synthesis of layered zeotype precursor B-SSZ-70(P), structure directing agent diisobutylimidazolium hydroxide was systematically replaced with cetyltrimethylammonium hydroxide (CTAOH)

At low CTAOH concentrations in the zeotype synthesis gel, CTA caps the zeotype external surface of the resulting B-SSZ-70(P), thereby limiting crystallite growth

At high CTAOH concentrations in the zeotype synthesis gel, swelling of the resulting B-SSZ-70(P) occurs

Delamination of the resulting materials via high-shear mixing is effective for CTA-capped materials and not effective for swollen materials

When functionalized with titanium, the delaminated CTA-capped materials are highly active olefin epoxidation catalysts

Competing Interest statement

The authors of the manuscript entitled "*Substitution of Cetyltrimethylammonium for OSDA Cations During B-SSZ-70 Zeotype Synthesis and Its Influence on Delamination*" have no competing interests to declare.